Hyperbolic dual finite volume models for shallow water flows in multiply-connected open channel networks

○ Hidekazu Yoshioka, Doctoral Student (Research Fellow of Japan Society for the Promotion of Science), Graduate School of Agriculture, Kyoto University, Kitashirakawa-Oiwake-cho, Sakyo-ku, Kyoto 606-8502, Japan, yoshih@kais.kyoto-u.ac.jp
Koichi Unami, Associate Professor, Graduate School of Agriculture, Kyoto University, Kitashirakawa-Oiwake-cho, Sakyo-ku, Kyoto 606-8502, Japan, unami@adm.kais.kyoto-u.ac.jp
Masayuki Fujihara, Professor, Graduate School of Agriculture, Kyoto University, Kitashirakawa-Oiwake-cho, Sakyo-ku, Kyoto 606-8502, Japan, fujihara@kais.kyoto-u.ac.jp

Shallow water flows in multiply-connected (looped) open channel networks are encountered in various surface water systems. Numerical simulation of such flows is one of the most important issues in environmental hydraulics and other related research fields. This paper presents two numerical models of shallow water flows, dynamic wave equations and local inertial equations, in which junctions are implicitly and efficiently handled. Mathematical properties of the two models are briefly reviewed in order to understand behaviour of their solutions. Computational results of test and real problems reveal their applicability and limitations for flows in open channel networks.

1. Introduction

Analysis of flows in surface water systems concerns a wide range of important problems in environmental hydraulics and other related research fields. Examples are flows in irrigation and drainage systems[1-2], flash floods propagating downstream valleys[3-4] and tidal flows in estuarine systems[5-6]. Macroscopic dynamics of these flows is reasonably described with the cross-sectionally averaged one-dimensional shallow water equations (1-D SWEs) assuming both the incompressibility of water and hydrostatic pressure distribution[7-8]. The 1-D SWEs are a coupled system of nonlinear hyperbolic partial differential equations having source terms. The 1-D SWEs cannot reproduce essentially multi-dimensional and non-hydrostatic phenomena that the 2-D and 3-D hydrodynamic models appropriately handle[9-10], such as solitary waves, breakings waves and oblique hydraulic jumps. Nevertheless, they have served as one of the most effective tools for engineering purposes because of their efficiency. Since analytical and approximate solutions to the 1-D SWEs are available only for limited cases, such as dam break problems in flat channels[11-12], numerical models have been used to solve them in scientific and engineering applications.

Several types of shallow water models including the 1-D SWEs have been presented so far. In this paper, the 1-D SWEs retaining the momentum flux term[13] are referred to as the dynamic wave equations (DYNs) in order to distinguish them from reduced counterparts. Examples of the reduced models are the local inertial equations (LOCs), the diffusion wave equation (DIF) and the kinematic wave equation (KIN)[14-17]. These models are derived with neglecting the temporal and/or momentum flux terms in the momentum equation while maintaining the complete mass conservation property. Although they cannot reproduce some important transient phenomena involving discontinuous water surface profiles that the 1-D SWEs deal with, their simplicity and higher efficiency are attractive in practical applications.

Typical surface water system presents a network structure, and is regarded as a connected graph consisting of a number of junctions connected with nodes (locally 1-D open channel networks)[18]. In real problems, shallow water flows in multiply-connected (looped) open channel networks are frequently encountered. Development of an efficient modeling framework for analyzing such flows is therefore an important issue. Since a connected graph has singularities at junctions where spatial derivatives and some hydraulic properties, such as discharge and cross-sectionally averaged velocity, are not well-defined. A key to develop a successful numerical model is to deal with junctions efficiently and consistently, which is achieved with the use of appropriate internal boundary conditions (IBCs) that describe balance laws of the mass and momentum at junctions. Almost all of the existing models handle the flows in reaches and at junctions separately, resulting in the loss of efficiency[19-21]. The authors developed mathematical models of shallow water flows in multiply-connected open channel networks that handle junctions as implicit IBCs, which is directly incorporated into the numerical counterparts without complicated algorithms[13, 22]. Two temporally explicit numerical models for the DYNs have been developed, which are here refereed to be as the finite element/volume method (FEVM) that solves the continuity equation with the standard finite element scheme and the momentum equation with a cell-centered finite volume scheme[13], and the dual finite volume method (DFVM) that utilizes the staggered finite volume scheme[22]. The authors recently found that these numerical models can also be applied to the LOCs with dropping only the momentum flux term.

The purpose of this paper is to carry out theoretical and numerical analyses to investigate applicability and limitation of the DYNs and LOCs. These models are solved using the DFVM and applied to test and real problems. Dam break problems and tidal flows in multiply-connected open channel networks are considered as the test problems. As the real problems, flows in a hydromorphic drainage system and flows in a river network driven by flood tide are considered, both of which differ significantly with each other in conditions. Since no direct comparison of the DYNs and LOCs for flows in open channel networks has been carried out, this paper contributes to further understandings of these models.

The remainder of this paper is organized as follows. Concise introductions for the DYNs and LOCs are given in Section 2. The DFVM is presented in Section 3. Test and real problems are carried out in Sections 4 and 5, respectively. Section 6 provides conclusions.

2. Shallow water models

2.1 Dynamic wave equations (DYNs)

The DYNs used in this paper consist of the continuity equation

$$\frac{\partial A}{\partial \eta}\frac{\partial \eta}{\partial t}+\frac{\partial Q}{\partial x}-q=T\frac{\partial \eta}{\partial t}+\frac{\partial Q}{\partial x}-q=0 \quad (1)$$

and the momentum equation

$$\frac{\partial Q}{\partial t}+\frac{\partial}{\partial x}\left(\frac{\beta Q^2}{A}\right)+gA\left(\frac{\partial \eta}{\partial x}+S_{\mathrm{f}}\right)=0 \tag{2}$$

where t is the time, x is the 1-D abscissa taken along the channel, A is the cross-sectional area of flow, T is the top width of the water surface, η is the water surface elevation, Q is the discharge, q is the lateral inflow, g is the gravitational acceleration, β is the momentum coefficient defined as[23]

$$\beta=\frac{1}{A}\int_A\left(\frac{u}{V}\right)^2 \mathrm{d}A \tag{3}$$

where u is the velocity in the cross-section and V is the cross-sectionally averaged velocity. The condition $\beta \geq 1$ holds for arbitrary shallow water flows according to the definition (3). S_{f} is the Manning's friction slope term[24]

$$S_{\mathrm{f}}=\frac{n^2 Q|Q|}{A^2 R^{4/3}} \tag{4}$$

where n is the Manning's coefficient and R is the hydraulic radius. The DYNs comprise a system of conservative hyperbolic PDEs with source terms, which handle both gradually and rapidly varied flows[25-26]. Momentum exchange caused by lateral inflows is not considered in (2) because only right-angled lateral inflows are assumed in this paper. The Manning's coefficient n and the momentum coefficient β are taken as constant values in a domain.

2.2 Local inertial equations (LOCs)

The LOCs consist of the continuity equation (1) and the reduced momentum equation

$$\frac{\partial Q}{\partial t}+gA\left(\frac{\partial \eta}{\partial x}+S_{\mathrm{f}}\right)=0\,, \tag{5}$$

in which the momentum flux term is neglected. Being different from the LOCs used in the literatures[15, 17], that presented in this paper deal with flows with general cross-sections.

As noted in Yoshioka *et al.*[27], solutions to the LOCs and DIF subject to a same boundary condition coincide if they exist. According to De Almeida *et al.*[17], relative errors of water depths between the DYNs and LOCs are roughly proportional to the square of a Froude number. Because the LOCs do not consider the momentum flux term, it is not suited to predict flows with a large Froude number such that junctions and channel bends are present where non-negligible horizontal exchanges of the momentum is important.

2.3 Eigenstructures

Eigenstructures of the DYNs and LOCs are presented in this sub-section for the purpose to briefly review their differences. The DYNs have the two eigenvalues

$$\lambda^{\pm}=\beta\frac{Q}{A}\pm\sqrt{\beta(\beta-1)\left(\frac{Q}{A}\right)^2+\frac{Ag}{T}}\,. \tag{6}$$

Assuming a cross-sectionally uniform flow ($\beta=1$) reduces (6) to the conventional ones

$$\lambda^{\pm}=\frac{Q}{A}\pm\sqrt{\frac{Ag}{T}}\,. \tag{7}$$

The eigenvalues $\lambda^{\pm}$ in (6) are rewritten using the "conventional" Froude number $F_{\beta=1}$ as

$$\lambda^{\pm}=\sqrt{\frac{Ag}{T}}\left(F_{\beta=1}\pm\sqrt{\frac{\beta-1}{\beta}\left(F_{\beta=1}\right)^2+1}\right), \tag{8}$$

which suggest the use of the "new" Froude number

$$F_{\beta}=\frac{F_1}{\sqrt{\dfrac{\beta-1}{\beta}F_1^2+1}} \tag{9}$$

where $F_{\beta=1}$ in (8) is described as F_1. Local flow regimes for the DYNs are summarized on the basis of F_{β} as follows:

- Subcritical flow ($F_{\beta}^2<1$),
- Critical flow ($F_{\beta}^2=1$),
- Supercritical flow ($F_{\beta}^2>1$).

The above classification for the flow regimes is equivalent to

- Subcritical flow ($F_1^2<\beta$),
- Critical flow ($F_1^2=\beta$),
- Supercritical flow ($F_1^2>\beta$).

If β is specified to be less than 1[28], $\lambda^{\pm}$ become complex under some conditions and then the DYNs loss the hyperbolicity.

As shown in the above, the momentum coefficient β plays a central role in determining the wave speeds. Since in practice cross-section of channel does not always have an idealized shape such as a rectangle, the value of β should be appropriately estimated. It is therefore recommended in applications to carry out a sensitivity analysis on it.

It is also important to note influences of β on solutions to problems with wet and dry interfaces. Among them, classical dry dam break problems have long been studied by many researchers in particular since the fundamental theoretical analysis of Ritter[29] who obtained the analytical expression of the front propagation speed of the wet and dry interfaces[30-33]. Hogg and Pritchard[33] analyzed problems with $\beta>1$ on the basis of the characteristics theory and showed that a wet and dry interface becomes ill-defined within a finite time if the friction slope is neglected in (2). This is due to the fact that the propagation speed of the disturbance exceeds that of the interface at the time, which is not a physically accepted situation.

The LOCs have the following two eigenvalues

$$\lambda^{\pm}=\pm\sqrt{\frac{Ag}{T}}\,, \tag{10}$$

which are formally derived with substituting $\beta=0$ into (6). According to (6) and (10), both the DYNs and LOCs are hyperbolic. As shown in (10), the wave celerity for the LOCs is slower than that of the DYNs. Furthermore, being different from the DYNs, solutions to the LOCs do not have critical and super-critical type flow regimes, indicating that they cannot reproduce transitional phenomena, such as hydraulic jumps and wet dam break problems.

2.4 Some remarks on the LOCs

This sub-section describes important remarks on the LOCs and DIF, the latter being a doubly-nonlinear degenerate parabolic PDE[16]. An apparent difference between the LOCs and DIF is that the temporal term in the momentum equation is neglected or not. Bates and his co-workers persist that the LOCs are superior to the DIF in the sense that an efficient numerical model can easily be developed for the former owing to fully retaining the temporal terms[15, 17]. This is because the latter in general requires the use of a very small time increment for temporally explicit method and a time-consuming iterative algorithm for implicit method.

Another remark to be noted is a relationship between the LOCs and DIF in an asymptotic limit. According to the theory of Chapman-Enskog expansion for singular hyperbolic PDEs[34], formally introducing a small parameter $0 < \varepsilon \ll 1$ in (5) yields

$$\varepsilon \frac{\partial Q}{\partial t} + gA\left(\frac{\partial \eta}{\partial x} + S_{\mathrm{f}}\right) = 0 . \tag{11}$$

Taking the limit of $\varepsilon \to +0$ in (11) leads to the DIF, a parabolic system of PDEs consisting of the continuity equation (1) and

$$\frac{\partial \eta}{\partial x} + S_{\mathrm{f}} = 0 . \tag{12}$$

Application of an asymptotic-preserving scheme[35] to (1) and (11) with a sufficiently small ε yields the approximate solution of the DIF with numerically retaining the temporal term of (11), which is far efficient compared with directly solving the DIF. This research topic is beyond the scope of this paper and will be addressed in future researches.

3. Dual finite volume method (DFVM)

In this paper, the DYNs and LOCs are solved using the DFVM (Appendix), a recently developed simple and versatile numerical method for shallow water flows both in single open channels and in open channel networks that have channel bends and multiply-connected structures. The DFVM applies a node-centered finite volume scheme to the continuity equation (1) and an upwind, cell-centered finite volume scheme to the momentum equation (2), respectively. The water surface elevation η and the discharge Q serve as the dependent variables, which are distributed to the dual cells and regular cells respectively. The dual cell is the 1-D counterpart of the Voronoi diagram for multiple dimensions. Upwind algorithms applied to the momentum flux and source terms stabilize numerical solutions without explicitly adding artificial dissipation terms. The DFVM does not require the use of water surface reconstruction algorithms to preserve a still water condition because it utilizes the water surface elevation η as a dependent variable. Local mass conservation at junctions is achieved as the implicit IBCs that do not rely on complicated numerical algorithms.

In this paper, the DFVM is slightly modified so that the upwinding of the momentum flux term in (2) is carried out with the new Froude number F_β not with the conventional one F_1. In the original DFVM, local flow regimes are identified from the value of F_1, which is not consistent with the eigenstructures of the DYNs as indicated in the previous section. According to preliminary numerical tests not presented in this paper, the modification does not significantly improve solution profiles; however, it certainly enhances theoretical foundations of the DFVM. In addition to the above modification, a new momentum flux evaluation scheme to more accurately simulate flows around junctions is implemented in the spatial discretization procedure[36]. Incorporation of the scheme into the DFVM significantly improves the accuracy to predict the discharge ratios for the flows downstream of a junction. The accuracy in some cases is comparable to that of a horizontally 2-D shallow water model, demonstrating its validity[37-38]. Performances of the DFVM have been verified with a series of benchmark tests of subcritical, supercritical and transcritical flows[39-42], clearly showing that it is as accurate as the other recently developed numerical models. The FEVM, a finite/element counter part of the DFVM, has also successfully been applied to a wide range of problems[13, 35, 43].

Application of the DFVM to the LOCs presented in this paper is straightforward because it is achieved simply neglecting the momentum flux term of (2). Spatial discretization for the other terms is carried out in a similar manner. Since the LOCs do not have the momentum flux term in its formulation, no momentum flux evaluation scheme is necessary in order to solve them in locally 1-D open channel networks.

Temporal integration of the DFVM is carried out using the classical fourth-order Runge-Kutta method. Since this temporal integration method is of an explicit type, the time increment Δt has to be chosen as a sufficiently small value[44] such that

$$\frac{\Delta x}{\Delta t} > \beta|V| + \sqrt{\beta(\beta-1)V^2 + \frac{Ag}{T}} , \tag{13}$$

where Δx is the elemental length is at least satisfied in an entire computational domain.

4. Test problems

Since the DFVM has been extensively verified with test problems in open channels, this paper focuses mainly on those of in open channel networks. An exception is the dam break problems firstly carried out in this section to see influences of β on solutions to the DYNs.

4.1 Dam break problems in a single channel

Dam break problems in an open channel serve as fundamental test cases to examine ability of a numerical model for the DYNs to resolve upstream and downstream wave propagations involving transitions and shocks. Here dam break problems in a straight, flat channel are considered. A 2,000 (m) length open channel is considered as the domain $\Omega = (0, 2000)$ (m). Cross-section of the channel is a rectangle with the width of 1 (m). The initial water elevation η (m) is specified as

$$\eta = \begin{cases} h_{\mathrm{U}} & (x \le 1000) \\ h_{\mathrm{D}} & (x > 1000) \end{cases} \tag{14}$$

where h_{U} (m) and h_{D} (m) denote the initial upstream and downstream water depths, respectively. The initial discharge is $Q = 0$ (m^3/s) in the entire Ω. The initial upstream water depth h_{U} is fixed to 10 (m), while the initial downstream water depths h_{D} are considered three cases: 5.0 (m) (Case DBA), 0.1 (m) (Case DBB) and 0.0 (m) (Cases DBC and DBD). Cases DBA and DBB are the problems in a frictionless channel, which intend to reveal dependence of the water surface profiles on β. On the other hand, in Cases DBB and DBC, non-zero Manningôs coefficient n are specified as 0.005 (s/$m^{1/3}$) in Case DBC and 0.020 (s/$m^{1/3}$) in Case DBD, respectively, both of which are realistic values in experimental and fields situations. The upstream and downstream boundaries of Ω are solid walls where flows are reflected. Ω is uniformly discretized into 2,000 regular cells so that numerical solutions sufficiently converge. The time increment Δt is fixed to 0.0015 (s).

The computed water surface profiles are illustrated in **Figs. 1** through **4** for each case with different values of β, namely, $\beta = 1.00$, 1.05, 1.10, 1.15 and 1.20. The label ñDBA-1.00ò represents the water surface profile in Case DBA for the value of $\beta = 1.00$, and so is for the others. **Figs. 1** and **4** show that the propagation speeds of the shocks and wet and dry interfaces increase as β increases. **Figs. 1** and **2** show that water depth immediately upstream of the shocks decrease smaller as β increases. **Figs. 3** and **4** indicate that the water surface profiles are apparently less sensitive to β in Cases DBC and DBD than those in the wet channel bed counterparts, but its influence is more significant for the smaller n. Although not presented here, specifying $n = 0$ (s/$m^{1/3}$) in a dry dam break problem results in a numerical failure being consistent with the theoretical results of Hogg and Pritchard[33].

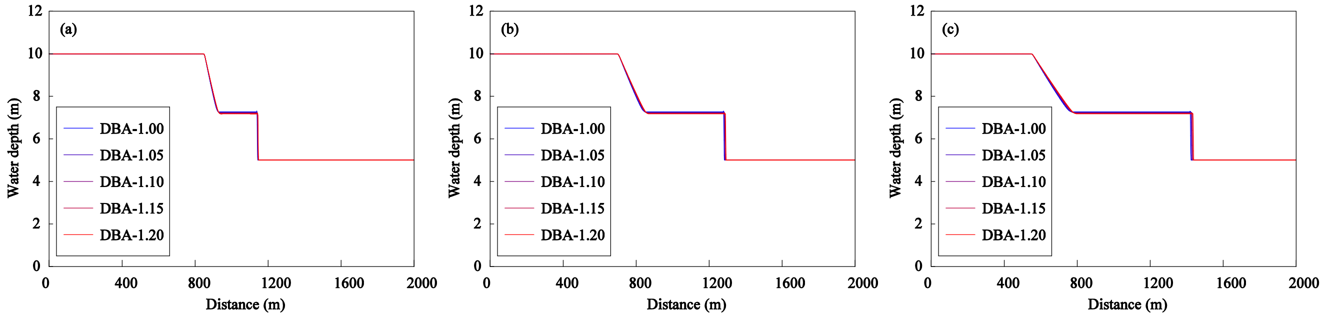

Fig. 1 Computed water surface profiles for Case DBA ((a) $t = 15$ (s), (b) $t = 30$ (s) and (c) $t = 45$ (s))

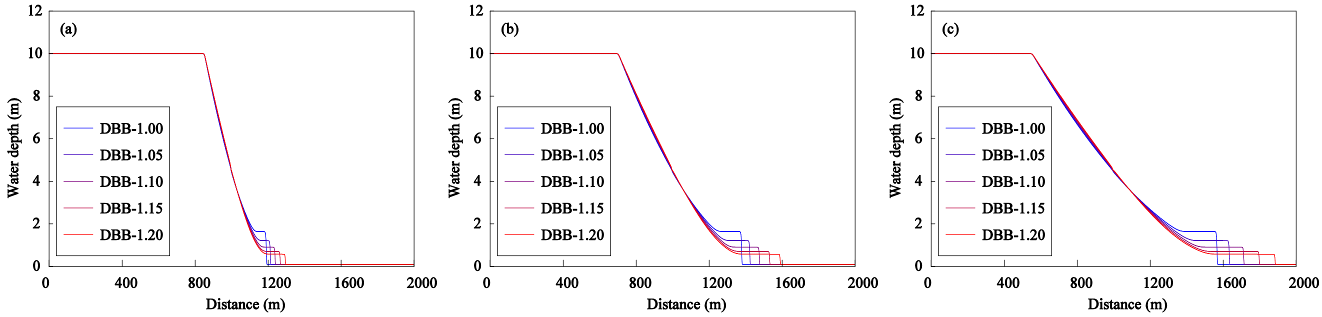

Fig. 2 Computed water surface profiles for Case DBB ((a) $t = 15$ (s), (b) $t = 30$ (s) and (c) $t = 45$ (s))

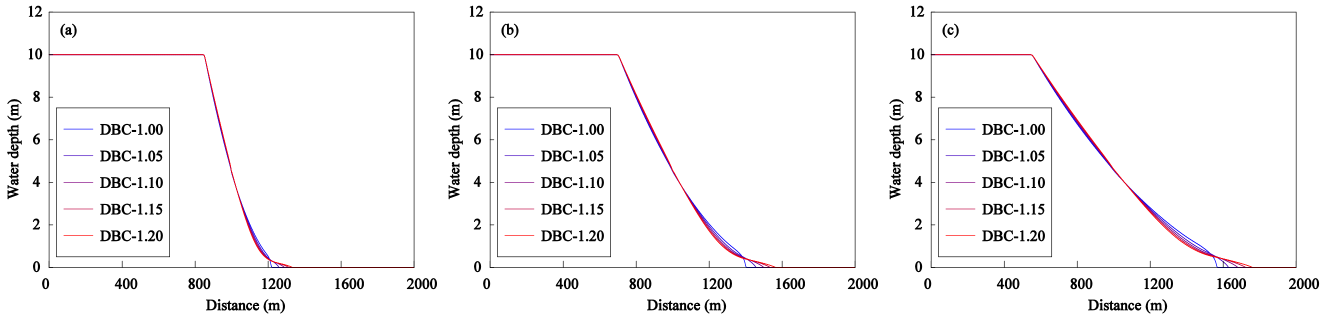

Fig. 3 Computed water surface profiles for Case DBC ((a) $t = 15$ (s), (b) $t = 30$ (s) and (c) $t = 45$ (s))

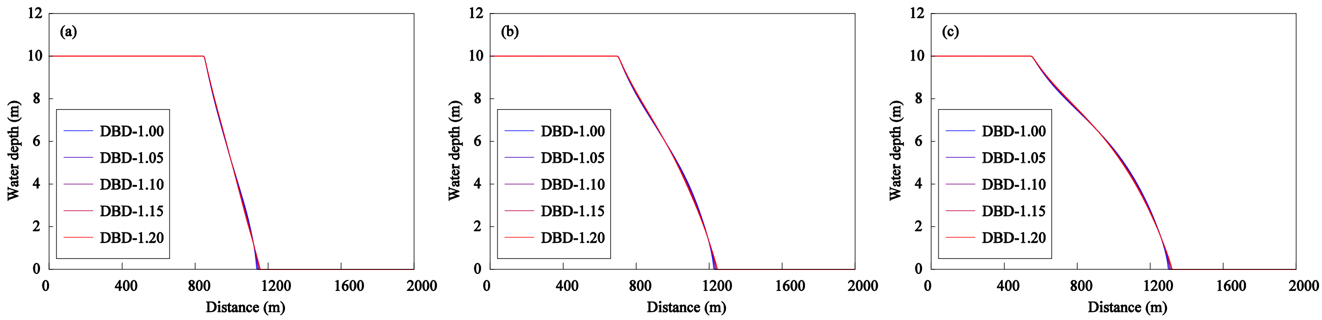

Fig. 4 Computed water surface profiles for Case DBD ((a) $t = 15$ (s), (b) $t = 30$ (s) and (c) $t = 45$ (s))

4.2 Dry dam break problem in an open channel network

A dry dam break problem in a hypothetical multiply-connected open channel network (**Fig. 5**) is carried out with the DYNs. This test problem is challenging because it requires a consistent junction treatment technique as well as a stable discretization method for rapidly varying transcritical flows involving wet and dry interfaces, non-rectangular cross-sections and channel bends. Only a few attempts at cross-sectionally averaged modeling have been made for the problems in open channel networks.

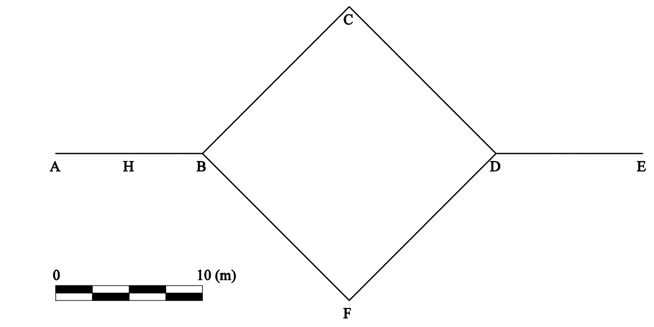

Fig. 5 Open channel network for test problems

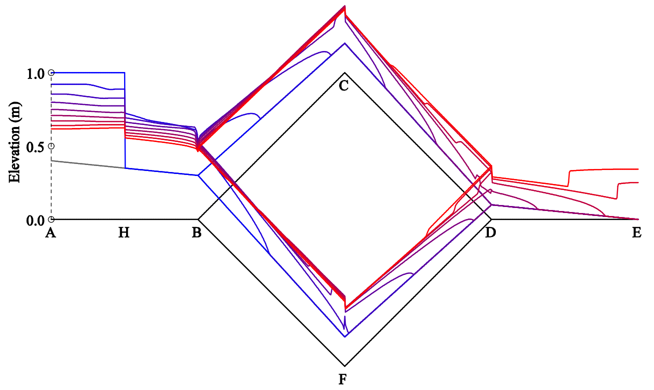

Fig. 6 Water surface profiles in the open channel network for the DYNs presented at the time interval of 5 (s)

The reaches in the channel network are equal in terms of length and bed slope, which are 10 (m) and 0.01, respectively. Cross-section of the channel is a rectangle with the width of 10 (m) in the reach A-H and a triangle with the side slope of 1:1 in the others. Manningôs coefficient n is set as 0.040 (s/m$^{1/3}$) for the reaches B-C-D and 0.030 (s/m$^{1/3}$) for the others. The momentum coefficient β is set as 1.1. A vertical wall serving as a dam is installed at the middle of reach A-B, namely H, dividing the channel network into an upstream reservoir (A-H) and a downstream multiply-connected channel network. The initial water depth immediately upstream of the dam is set as 0.6 (m) and the downstream channel network is initially dry. Both the upstream and downstream-ends are solid walls. The dam is instantaneously removed at the initial time $t=0$ (s). Each reach is divided into 200 regular cells. The time increment Δt is set as 0.001 (s).

Fig. 6 shows the computed water surface profiles in the domain. A surge from the reservoir separates at B. The divided surges converge at D and hit the downstream wall at E, generating a receding bore propagating upstream. There are also other receding bores starting at bending points C and F, as observed in some experiments[45]. Increasing spatial and temporal resolutions do not significantly alter the computational results, showing validity of the numerical simulation carried out here.

The LOCs has also been applied to this problem; however, the computed water surface profile diverged, highly oscillating around the dam H. This is considered due to the instability of the DFVM for the LOCs, indicating necessity of improvements.

4.2 Tidal flows in an open channel network

The DYNs and LOCs are next applied to numerical simulation of tidal flows in a hypothetical flat, multiply-connected open channel network. The domain has a same network structure with the locally 1-D open channel network used in the previous test problem. Length of each reach is 1,000 (m). Cross-section of the channel is a rectangle with the width of 25 (m) for all the reaches. The momentum coefficient β is set as 1.1. The boundary E is a solid wall. The boundary A is treated as an open boundary at which the water surface elevation η_{A} is specified directly using a sinusoid function as

$$\eta_{\mathrm{A}}=5+\sin\left(\frac{2\pi t}{43,200}\right). \tag{15}$$

Initial condition is set as a still water with the water depth of 5 (m). Each reach is divided into 200 regular cells. The time increment Δt is set as 0.5 (s). Terminal time of the computation is 43,200 (s).

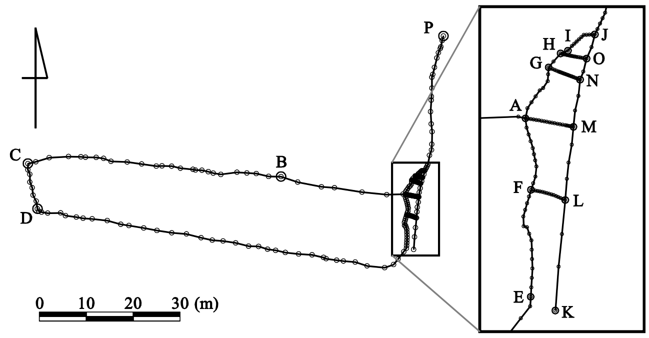

Fig. 7 Computational domain for the first real problem

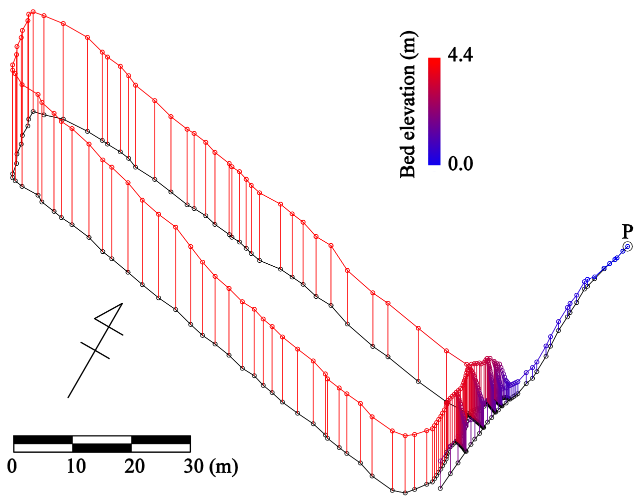

Fig. 8 Bed elevation distribution in the domain

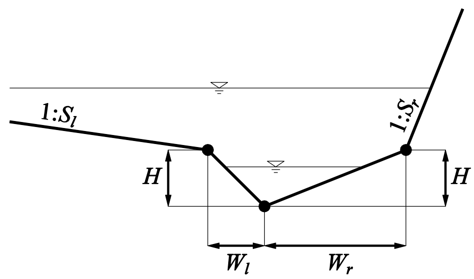

Fig. 9 A sketch of cross-section for the first real problem

Maximum relative errors between the computed water depths for the DYNs and LOCs at the key nodes B, C, D, E and F are 9.2×10^{-4}, 1.1×10^{-3}, 1.2×10^{-3}, 1.2×10^{-3} and 1.2×10^{-3}, respectively, demonstrating that the results of the two models are almost identical. This is because the Froude number of the flow is sufficiently small such that the use of the LOCs is justified. The results indicate applicability of the LOCs to numerical simulation of tidal flows in multiply-connected open channel networks with relatively wide channel widths.

5. Real problems

For the purpose of making further comparisons of the DYNs and LOCs, numerical simulations of two significantly different real shallow water flows in multiply-connected open channel networks are carried out.

5.1 Flows in a hydromorphic drainage system

Applicability of the DYNs and LOCs to real problems is firstly assessed with surface water flows in a multiply-connected open channel network draining hydromorphic farmlands in the Guinea savanna agro-ecological zone of Ghana[13, 46]. The main water input into the channel network is direct rainfall and lateral groundwater seepage from the surrounding rice fields. **Fig. 7** illustrates a plane view of the open channel network as the computational domain with the mesh and key nodes alphabetically labeled from A through P. The open channel network consists of a main loop (A-B-C-D-E-F-A) running in the rice fields, a downstream gully (K-L-M-N-O-J-P) and steep cliffs connecting the main loop and the gully (F-L, A-M, G-N, H-O and I-J). The node D is the highest point in the channel network, K and P the boundaries, A, F, G, H, J, L, M, N and O are junctions. The node P is the downstream-end of the domain where a free-overflow natural weir is installed. **Fig. 8** shows bed elevation distribution in the domain where that of the downstream-end P is set as the normal elevation 0 (m). Bed slopes in the domain are very irregular with the maximum value of 1/2.14 in a gully. Cross-section of the channel is non-rectangular and non-prismatic, which is governed by the five parameters H, W_l, W_r, S_l and S_r as shown in **Fig. 9**[13]. Total numbers of the regular cells and the nodes in the computational domain are 228 and 224, respectively. Yoshioka *et al.*[18, 47] computed mean residence time distribution of a conservative solute injected into the domain on the basis of Kolmogorovὂs backward equations, estimating the maximum mean residence time of the solute in the domain as 2,200 (s) at a no-rainfall steady state and as 500 (s) that of during the rainfall event focused on later, respectively.

The momentum coefficient β and the Manningὂs coefficient n in the domain have been estimated as 1.10 and 0.015 (s/m$^{1/3}$), respectively[13]. Surface water flows in the channel network exhibit highly complicated natures including both subcritical and supercritical flows due to its irregular topography. The time increment is set as $\Delta t = 0.05$ (s). Other computational conditions are same with those in Unami and Alam[13].

Fig. 10 presents computational results of the outflow hydrographs at the downstream-end P for the DYNs and LOCs during a rainfall event in a rainy season that caused severe þoods in downstream area of the farmlands. The outflow discharge of the LOCs is gently varying compared with that of the DYNs. Maximum relative error between the discharges for the models is more than 0.4.

Another set of numerical simulations for the DYNs are also carried out under the same initial and boundary conditions with varying the values of the momentum coefficient β for the purpose of a brief sensitivity analysis. Computational results of the relative errors for the outflow discharge at the downstream-end P are shown in **Fig.11**. The label ñRelative error-1.00ò represents the relative error of the outflow

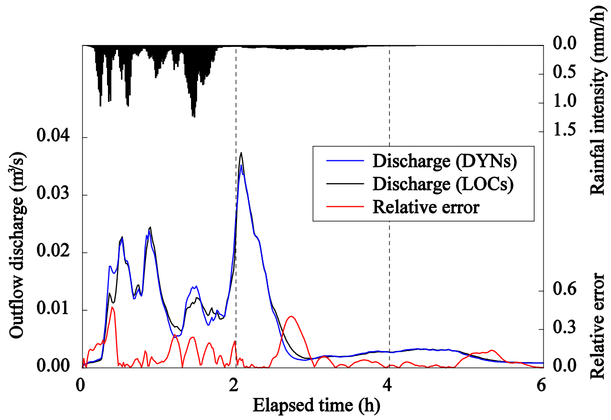

Fig. 10 Computed outflow discharges at P for the DYNs and LOCs and the relative errors between them

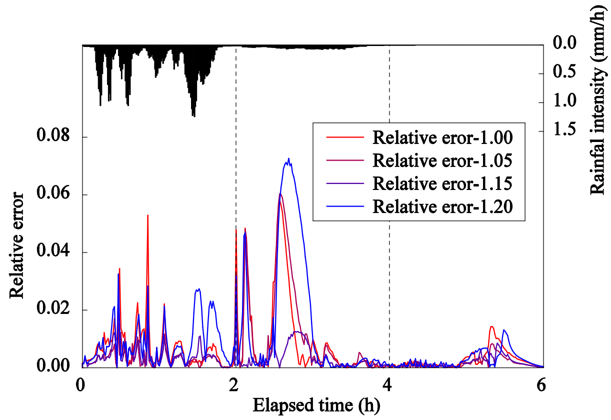

Fig. 11 Computed outflow discharges at P for the DYNs with different values of the momentum coefficient β

discharges between that of the estimated value $\beta = 1.10$ and that of $\beta = 1.00$, and so is for the others. Maximum value of the relative error is less than 0.08 for these computational cases, showing that varying β within the presented range does not significantly alter the hydrograph.

5.2 Flows in a river network driven by a flood tide

The DYNs and LOCs are next applied to numerical simulation of flows driven by a flood tide in a tidal river network surrounding a polder near the coast of Bay of Bengal, Bangladesh[48]. **Fig. 12** illustrates a plane view of the river network as the computational domain with labeled key nodes. The river network is connected with Bay of Bengal at B-0. The boundary B-1 is connected with one of the downstream tributaries of the Meghna River. A polder surrounded by tidal river is vulnerable to flood tides that may cause a severe flooding events associating salt damages[49-50]. In these coastal areas, such a serious event is caused by the arrival of a tropical typhoon. Shallow water models can serve as the foundation of effective analysis of this kind of disasters.

The river network is discretized into a mesh with 398 regular cells and 394 nodes. The normal water level is set as 0 (m) above the sea level. Channel bed elevation in the large river network surrounding the polder is set as -10 (m), while those for the small channels in the polder are distributed between -4 (m) and 0 (m). A still water with the surface water elevation of 0 (m) in the entire domain is set as the initial condition. The two boundaries B-0 and B-1 are open boundaries at which the external water surface elevation η_{E} for a hypothetical flood tide event is specified as[48]

$$\eta_{\mathrm{E}} = \max\left(0, 5\min\left(\frac{t}{43,200}, \frac{86,400-t}{43,200}\right)\right) \text{ (m).} \qquad (16)$$

The discharge at the open boundaries B-0 and B-1 are specified on the basis of η_{E} as

$$Q_{\mathrm{E}} = T_{\text{B-0 or B-1}} \left|\eta_{\text{B-0 or B-1}} - \eta_{\mathrm{E}}\right| \sqrt{2g\left|\eta_{\text{B-0 or B-1}} - \eta_{\mathrm{E}}\right|} \text{ (m}^3\text{/s).} \qquad (17)$$

The other boundaries are treated as solid walls. The time increment is set as $\Delta t = 1$ (s).

Figs. 13 and **14** show the computed water surface elevations in the river network at the peak ($t = 43,200$ (s)) and at the end ($t = 86,400$ (s)) of the flood tide for the DYNs and LOCs, respectively. Relative errors between the water surface elevations at the peak and end of the flood tide are 1.1×10^{-2} and 7.7×10^{-3}, respectively, showing that the LOCs give comparative computational results with the DYNs at the peak. The computed water surface elevations for the LOCs are less than those of the DYNs, indicating that application of the former to analysis of a flood tide event results in an underestimation of its risk.

Although the simulation has successfully been carried out without numerical failures, it should be emphasized that the DFVM presented in this paper computes flows only in the channels. Overtopping flows from the channels to the polders are therefore not taken into account. More realistic, detailed numerical simulations of flood tides require the use of a sophisticated coupled modelling framework of water flows both in cross-sectionally 1-D open channel flows and horizontally 2-D overland flows[51-52]. An FEVM for solving the 2-D SWEs currently under development can be used for this purpose[53].

6. Conclusions

Two shallow water models, the DYNs and LOCs, are presented and applied to test and real problems in order to investigate their applicability and limitations. Several mathematical properties of the DYNs and LOCs were briefly reviewed mainly focusing on their eigenstructures. Computational results of the test and real problems for the DYNs with the DFVM demonstrated their versatility, well reproducing the numerical solutions without numerical failures under the severe computational flows. The computational results also suggested high applicability of the LOCs to analysis of the flows in multiply-connected tidally-driven river networks where the Froude number is sufficiently small. The results were comparable to those of with the DYNs. On the other hand, the computational results of the dam break problems showed clearly that the present LOCs should not be applied to simulate these kinds of flows. In conclusions, the LOCs give reasonable results for the flows with small Froude numbers where the momentum exchanges are negligible.

As demonstrated in this paper, the DFVM, a fully explicit numerical model for the DYNs and LOCs, has successfully been applied to numerical simulations under various flow conditions. Computational performance of the DFVM can be improved if a semi-implicit algorithm is incorporated into it in order to remove the restriction for the time increment. Then the improvements should be made so that its algorithmic simplicity is not degraded. There remain many important research topics to be addressed in order to develop a more promising model for analyzing a wide range of shallow water flows, such as coupling of the DYNs with multi-dimensional shallow water models or with groundwater flow models[54-55]. The DFVM used in this paper will be applied to risk analysis of a catastrophic dam break flash flood in Japan caused by a huge earthquake, and the analysis results will be presented in elsewhere.

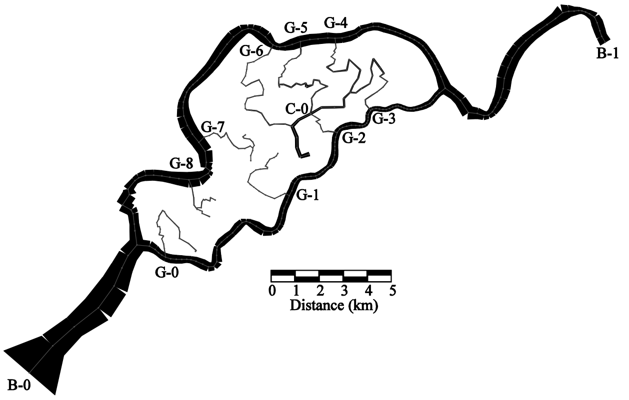

Fig. 12 Computational domain for tidal flows in an estuary

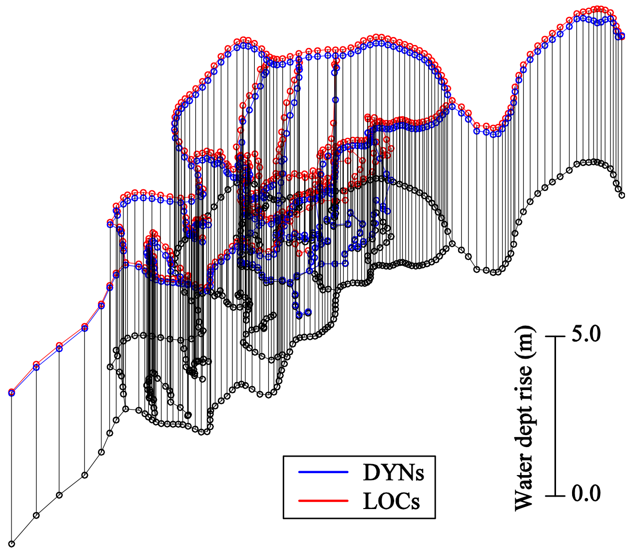

Fig. 13 Computed water surface profiles for the DYNs and LOCs at the peak of the flood tide

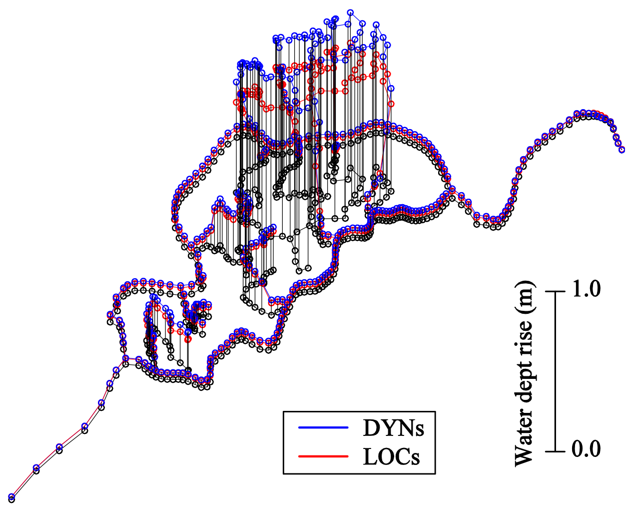

Fig. 14 Computed water surface profiles for the DYNs and LOCs at the end of the flood tide

Acknowledgement

This paper is financially supported by the JSPS under grant 25・2731.

Appendix

Spatial discretization algorithm for the DFVM used in this paper is described in this appendix.

A.1 Computational mesh

A couple of staggered computational meshes, a regular mesh and a dual mesh, are used in the DFVM. The continuity equation (1) is solved on the dual mesh, while the momentum equation (2) on the regular mesh, so as to avoid conflicting numbers of equations and unknowns. The domain Ω is first divided into a regular mesh consisting of regular cells bounded by two nodes, so that a junction falls on one of the nodes. The regular cells and the nodes are indexed with the natural numbers. The total numbers of regular cells and nodes are denoted by N_{c} and N_{n}, respectively. The *k*th regular cell is denoted by Ω_k. The length of Ω_k is represented by l_k. The two nodes bounding both sides of Ω_k are denoted by the $\varphi(k,1)$ th node and the $\varphi(k,2)$ th node. The abscissa in Ω_k is directed to the $\varphi(k,2)$ th node. The number of regular cells connected to a generic *i*th node is denoted by $\nu(i)$. The *j*th regular cell connected to the *i*th node is referred to as the $\kappa(i,j)$ th regular cell $\Omega_{\kappa(i,j)}$. There are two nodes that bound $\Omega_{\kappa(i,j)}$. One is the *i*th node, and the other is referred to as the $\mu(i,j)$ th node. In $\Omega_{\kappa(i,j)}$, the direction of the abscissa is identified with the parameter $\sigma_{i,j}$, which equals 1 when x is directed to the $\mu(i,j)$ th node, and otherwise to -1. A dual mesh is generated from the regular mesh. Following the multi-dimensional analogue of Mishev[56], define the *i*th dual cell S_i as

$$S_i = \left\{ x \middle| \, |x_i - x| < \left| x_{\mu(i,j)} - x \right| \ \text{ for } \ 1 \le j \le \nu(i) \right\} \tag{18}$$

where x_i and $x_{\mu(i,j)}$ represent x at the *i*th node and at the $\mu(i,j)$ th node, respectively. The dual mesh consists of N_{n} dual cells. The cell interface between S_i and $S_{\mu(i,j)}$ is denoted by $\Gamma_{i,j}$. The water elevation η is attributed to the dual cells, and the discharge Q to the regular cells. The discretized η in S_i is denoted by η_i, and the discretized Q in Ω_k by Q_k.

A.2 Continuity equation

The continuity equation (1) is discretized on a dual mesh. The cell-vertex finite volume formulation of the continuity equation in the dual cell S_i is

$$\int_{S_i} T \frac{\partial \eta}{\partial t} \mathrm{d}x + \sum_{j=1}^{\nu(i)} \sigma_{i,j} Q_{\kappa(i,j)} = \int_{S_i} q \mathrm{d}x \, . \tag{19}$$

Assuming a linear variation of the top width T in $\Omega_{\kappa(i,j)}$ yields the following relationship

$$T = T_{i,j,0} + \frac{x - x_i}{\sigma_{i,j} l_{\kappa(i,j)}} \left(T_{i,j,1} - T_{i,j,0} \right) \tag{20}$$

where $T_{i,j,0}$ and $T_{i,j,1}$ are the values of T at the *i*th node and at the $\mu(i,j)$ th node in $\Omega_{\kappa(i,j)}$, respectively. The first term on the left-hand side of (19) is evaluated as

$$\int_{S_i} T \frac{\partial \eta}{\partial t} \mathrm{d}x = \left(\frac{1}{8} \sum_{j=1}^{\nu(i)} l_{\kappa(i,j)} \left(3T_{i,j,0} + T_{i,j,1} \right) \right) \frac{\mathrm{d}\eta_i}{\mathrm{d}t} \, , \tag{21}$$

leading to

$$\frac{\mathrm{d}\eta_i}{\mathrm{d}t} = \left(-\sum_{j=1}^{\nu(i)} \sigma_{i,j} Q_{\kappa(i,j)} + \sum q \right) \Bigg/ \left(\frac{1}{8} \sum_{j=1}^{\nu(i)} l_{\kappa(i,j)} \left(3T_{i,j,0} + T_{i,j,1} \right) \right) \tag{22}$$

where $\sum q$ represents the discharge contributed from the lateral inflows and the boundary conditions.

A.3 Momentum equation

The upwind FVM[13] based on the local Froude number is applied to the momentum equation (2). The cell-centered finite volume formulation of the momentum equation in Ω_k leads to

$$l_k \frac{\mathrm{d}Q_k}{\mathrm{d}t} + \left[F \right]_{\partial\Omega_k} = \int_{\Omega_k} gA \left(-\frac{\partial \eta}{\partial x} - S_{\mathrm{f}} \right) \mathrm{d}x \tag{23}$$

where Ω_k is the interface of $\partial\Omega_k$.

Flux evaluation in the momentum equation (2) is carried out with a simple upwind discretization. For each generic regular cell Ω_k, the node, of the two nodes bounding Ω_k, to which the flow is directed is referred to as the downstream node, and the other is referred to as the upstream node. The vector starting from the upstream node and ending at the downstream node is denoted by χ_k. The cell flux F_k for the regular cell Ω_k is determined using the local Froude number as a weight. When the downstream node in Ω_k is wet, $A_{k,\mathrm{DS}} \ge \varepsilon$ for a small threshold value ε, and the cell cross-sectional area A_k and the cell cross-sectionally averaged velocity V_k are calculated as

$$V_k = \frac{Q_k}{A_k} \tag{24}$$

with the cell cross-sectional area

$$A_k = \left(1 - \omega_k \right) A_{k,\mathrm{DS}} + \omega_k A_{k,\mathrm{US}} \tag{25}$$

and the weight

$$\omega_k = \max \left(1 - \frac{1}{Fr_k^{\ 2}}, 0 \right) \tag{26}$$

where Fr_k^2 is the square of the cell local Froude number F_β in (9) computed using β, g, $T_{k,\mathrm{DS}}$, Q_k and $A_{k,\mathrm{DS}}$, and the subscripts US and DS indicate values at the upstream node and the downstream node, respectively, in Ω_k. The velocity V_k is taken to be 0 when $A_{k,\mathrm{DS}} < \varepsilon$. Finally, the cell flux F_k is determined as

$$F_k = \beta_k Q_k V_k \, . \tag{27}$$

The flux on the cell interface $\partial\Omega_k$ is evaluated considering connections between cells and the momentum balance principles[13, 35]. The set of indices of the regular cells, the downstream (upstream) nodes of which fall on the upstream (downstream) node of Ω_k, is denoted as U_k (D_k). The flux at the upstream cell interface $\partial\Omega_{k,\mathrm{US}} \subset \partial\Omega_k$ is prescribed as

$$F\big|_{\partial\Omega_{k,\mathrm{US}}} = \sum_{\kappa \in U_k} r_k \max\left(\cos\theta_{k,\kappa}, 0 \right) F_\kappa \tag{28}$$

where r_k is the discharge ratio defined analogues to that of Yoshioka *et al.*[36] as

$$r_k = \left| Q_k \right| \left(\sum_{\kappa \in D_k} \left| Q_\kappa \right| \right)^{-1} \tag{29}$$

which equals to 0 if its denominator vanishes and $\theta_{k,\kappa}$ is the angle between χ_k and χ_κ. The discharge ratio r_k satisfies the partition of unity property

$$\sum_{\kappa \in D_k} r_k = 1 \, . \tag{30}$$

The flux at the downstream cell interface $\partial\Omega_{k,\mathrm{DS}} \subset \partial\Omega_k$ is identical to the cell flux

$$F\big|_{\partial\Omega_{k,\mathrm{DS}}} = F_k \tag{31}$$

with the exception that

$$F\big|_{\partial\Omega_{k,\mathrm{DS}}} = F_k - \min\left(\cos\theta_{k,\kappa}, 0\right) F_\kappa \tag{32}$$

when the downstream node is connected to exactly two regular cells. Finally, the second term of the left-hand side of (23) is evaluated using $F\big|_{\partial\Omega_{k,\mathrm{US}}}$ and $F\big|_{\partial\Omega_{k,\mathrm{DS}}}$ with considering the directions of the flows as well as that of the x abscissa. The momentum flux evaluation scheme presented is physically relevant in the sense that it considers the contact angles of the channels meeting at a junction and guarantees non-increase of the momentum variation[57]. Application of an improper, momentum variation-increasing scheme to the DFVM leads to unphysical surface water profiles[36, 58].

The source terms in the right-hand side of (23) are discretized using an upwind algorithm. The first term of the right-hand side of (23) is evaluated as

$$\int_{\Omega_k} gA\left(-\frac{\partial\eta}{\partial x}\right)\mathrm{d}x = -gl_k\overline{A}_k\left(\eta_{\varphi(k,2)} - \eta_{\varphi(k,1)}\right) \tag{33}$$

with

$$\overline{A}_k = \begin{cases} A_{k,\mathrm{US}} & \left(Fr_k^{\ 2} \geq 1\right) \\ \dfrac{A_{k,\varphi(k,1)} + A_{k,\varphi(k,2)}}{2} & \left(Fr_k^{\ 2} < 1\right) \end{cases}. \tag{34}$$

The second term of the right-hand side of (23), the friction slope term, is discretized as

$$\int_{\Omega_k} gA\left(-S_\mathrm{f}\right)\mathrm{d}x = -gl_k\overline{A}_k S_{\mathrm{f},k} \tag{35}$$

with

$$S_{\mathrm{f},k} = \frac{n_k^2 Q_k\left|Q_k\right|\overline{P}_k^{\ 4/3}}{\overline{A}_k^{\ 10/3}} \tag{36}$$

and

$$\overline{P}_k = \begin{cases} P_{k,\mathrm{US}} & \left(Fr_k^{\ 2} \geq 1\right) \\ \dfrac{P_{k,\varphi(k,1)} + P_{k,\varphi(k,2)}}{2} & \left(Fr_k^{\ 2} < 1\right) \end{cases}. \tag{37}$$

However, S_f is taken as 0 when $\overline{A}_k < \varepsilon$. Finally, each $\dfrac{\mathrm{d}Q_k}{\mathrm{d}t}$ is explicitly computed as

$$\frac{\mathrm{d}Q_k}{\mathrm{d}t} = \frac{1}{l_k}\left(-\left[F\right]_{\partial\Omega_k} - g\overline{A}_k\left(\eta_{\varphi(k,2)} - \eta_{\varphi(k,1)} + l_k S_{\mathrm{f},k}\right)\right). \tag{38}$$

The system of ordinary differential equations (22) and (38) is solved using the Runge-Kutta method with appropriately specified initial and boundary conditions.

Bibliography

(1) Trancoso, A.R., Braunschweig, F., Leitao, P.C., Obermann, M. and Neves, R., ñAn advanced modeling tool for simulating complex river systemsò, *Sci. Total Environ*., 407(8) (2009). pp. 304-3016.

(2) Van Thang, P., Chopard, B., Lefèvre, L., Ondo, D.A. and Mendes, E., ñStudy of the 1D lattice Boltzmann shallow water equation and its coupling to build a canal networkò, *J. Comput. Phys*., 229(19) (2010), pp. 7373-7400.

(3) Carrivick, J.L., Manville, V., Graettinger, A. and Cronin, S.J., ñCoupled fluid dynamics-sediment transport modelling of a Crater Lake break-out lahar: Mt. Ruapehu, New Zealandò, *J. Hydrol*., 388(3-4) (2010), pp. 399-413.

(4) Yoshioka, H., Unami, K. and Fujihara, M., ñA dual grid based finite volume model for dam break flows in multiply connected open channel networks with general cross-sectionsò, *Proc. the 62nd Japan National Congress for Theoretical and Applied Mechanics*, 2013a, OS19-09, 2pp.

(5) Bushman, F.A., Hoitink, A.J.F., Van Der Vegt, M. and Hoekstra, P., ñSubtidal flow division at a shallow tidal junctionò, *Water Resour. Res*., 46 (2010), W12515, 12pp.

(6) Sassi, M.G., Hoitink, A.J.F., De Brye, Vermeulen, B. and Deleersnijder, E., ñTidal impact on the division of river discharge over distributary channels in the Mahakam Deltaò, *Ocean Dyn*., 61(12) (2011), pp. 2211-2228.

(7) Cunge, J.A., Holly Jr., F.M. and Verwey, A., *Practical Aspects of Computational River Hydraulics*, 1980, Pitman, pp. 7-52.

(8) Szymkiewicz, R., *Numerical Modeling in Open Channel Hydraulics*, Springer, 2010, pp.263-300.

(9) Yang, C., Lin, B., Jiang, C. and Liu, Y., ñPredicting near-field dam-break flow and impact force using a 3D modelò, *J. Hydraul. Res*., 48(6) (2011), pp. 784-792.

(10) Shinha, S., Liu, X. and Garcia, M.H., ñThree-dimensional hydrodynamic modeling of the Chicago River, Illinoisò, *Environ. Fluid Mech*., 12(5) 2012, pp. 471-494.

(11) Stoker, J.J., *Water waves*. Interscience publishing, New York, 1957, pp.291-341.

(12) Delestre, O., Lucas, C., Ksinant, P.A., Darboux, F., Laguerre, C., Vo, T.N.T., James, F. and Cordier, S., ñSWASHES: a compilation of shallow water analytic solutions for hydraulic and environmental studiesò, *Int. J. Numer. Methods Fluids*, 72(3) (2013), pp.269-320.

(13) Unami, K. and Alam, A.H.M.B., ñConcurrent use of finite element and finite volume methods for shallow water equations in locally 1-D channel networksò, *Int. J. Numer. Methods Fluids*, 69(2) (2012), pp. 255-272.

(14) Yen, B.C. and Tsai, C.W.S., ñOn noninertia versus diffusion wave in flood routingò, *J. Hydrol.*, 244(1-2) (2001), pp. 97-104.

(15) Bates, P.D., Horritt, M.S. and Fewtrell, T.J., ñA simple inertial formulation of the shallow water equations for efficient two-dimensional flood inundation modellingò, *J. Hydrol*., 387(1-2) (2010), pp. 33-45.

(16) Santillana, M. and Dawson, C., ñA numerical approach to study the properties of solutions of the diffusive wave approximation of the shallow water equationsò, *Comput. Geosci.*, 14(1) (2010), pp. 31-53.

(17) De Almeida, G.A.M. and Bates, P., ñApplicability of the local inertial approximation of the shallow water equations to flood modelingò, *Water Resour. Res*., 49 (2013), 12pp.

(18) Yoshioka, H., Unami, K. and Kawachi, T., ñPartial differential equation model for spatially distributed statistics of contaminant particles in locally one-dimensional open channel networksò, *Proc. Tenth International Conference on Hydroscience and Engineering*, (2012), 24pp.

(19) Colombo, R.M., Guerra, G., Herty, M., and Schleper, V. ñOptimal control in networks of pipes and canalsò, *SIAM, J. Control Optim*., 48(3) (2009), pp. 2032-2050.

(20) Marigo, A., ñEntropic solutions for irrigation networksò, *SIAM, J. Appl. Math*., 70(5) (2010), pp. 1711-1735.

(21) Herty, M. and Seaid, M., ñAssessment of coupling conditions in water way intersectionsò, *Int. J. Numer. Methods Fluids*, 71(11) (2012), pp. 1438-1460.

(22) Yoshioka, H. and Unami, K., ñA dual grid based finite volume

scheme for analysis of shallow water flows in locally one-dimensional open channel network flowsò, *Proc. the 69^{th} JSDIRE, Kyoto Division*, (2012), pp. 114-115. (in Japanese)

(23) Costabile, P. and Macchione, F., ñAnalysis of one-dimensional modelling for flood routing in compound channelsò, *Water Resour. Manage.*, 26(5) 2012, pp. 1065-1087.

(24) Yen, B.C., ñOpen channel flow resistanceò, *J. Hydraul. Eng*, 128(1) (2002), pp. 20-39.

(25) Lai, C., Baltzer, R.A. and Schaffranek, R.W., ñConservation-form equations of unsteady open-channel flowò, *J. Hydraul. Res.*, 40(5) (2002), pp. 567-578.

(26) GŃsiorowski, D., ñBalance errors generated by numerical diffusion in the solution of non-linear open channel flow equationsò, *J. Hydrol.*, 476 (2013), pp. 384-394.

(27) Yoshioka, H., Kinjo, N., Wakazono, A., Unami, K. and Fujihara, M., ñApplication of two shallow water models to steady flow analysis in a vegetated agricultural drainage canalò, *J. Rainwater Catch. Syst*. (under review)

(28) Abedini, M.J. and Hashemi, M.R., ñEffect of convective term suppression in numerical simulation of trans-critical open channel flowò, *Iranian J. Sci. Tech. Trans. B. Engrg*., 31(B1), pp. 85-96.

(29) Ritter, A., ñDie Fortpflanzung der Wasserwellenò, *Z. Vereines Deutsch. Ing.*, 36(33) (1982), pp. 947-954. (in German)

(30) Whitham, G.B., ñThe effects of hydraulic resistance in the dam-break problemò, *Proc. R. Soc. Lond.* A., 227 (1955), pp. 399-407

(31) Chanson, H., ñAnalytical Solutions of Laminar and Turbulent Dam Break Waveò, *Proc. of River Flow*, 2006, pp. 465-474.

(32) Chen, Y.C., Wu, B. and Wang, B., ñSimilarity solution of dam-break flow on horizontal frictionless channelò, *J. Hydraul. Res.*, 49(3) (2012), pp. 384-387.

(33) Hogg, A.J. and Pritchard, D., ñThe effects of hydraulic resistance on dam-break and other shallow inertial flowsò, *J. Fluid Mech*., 501 (2004), pp. 179-202.

(34) Liu, T.P., ñHyperbolic conservation laws with relaxationò, *Commun. Math. Phys*., 108(1) (1987), pp. 153-175.

(35) Berthon, C., Chalons, C. and Turpault, R., ñAsymptotic-preserving Godunov-type numerical schemes for hyperbolic systems with stiff and non-stiff relaxation termsò, *Numer. Methods Partial Differ. Equat*., 29(4) (2013), pp. 1149-1172.

(36) Yoshioka, H., Unami, K. and Fujihara, M., ñComparative numerical analysis on momentum flux evaluation schemes for shallow water flows in open channel networksò, *J. Rainwater Catch. Syst*. (in press)

(37) Ashida, K. and Kawai, S., ñHydraulic behaviors of dividing flow around junctionsò, *Disaster Prevention Research Institute Annuals*, 55 (1979), pp. 491-506. (in Japanese)

(38) Koseki, H., Hoshino, T. and Yasuda, H., ñStudy on distribution ratio in bifurcation of response to down stream boundary conditionò, *J. JSCE, Ser. B1*, 69(4) (2013), pp. I_601-I_606. (in Japanese)

(39) Goutal, N. and Maurel, F., *Proc. the 2nd Workshop on Dam-break Wave Simulation*, EDF-DER Report, HE-43/97/016/B, 1997.

(40) Vázquez-Cendón, M.L., ñImproved treatment of source terms in upwind schemes for the shallow water equations in channels with irregular geometryò, *J. Comput. Phys*., 148(2) (1999), pp. 11-34.

(41) Zoppou, C. and Roberts, S. ñExplicit schemes for dam-break flowsò, *J. Hydraul. Eng.*, 129(1) (2003), pp.11-34.

(42) Aricò, C., Sinagra, M. and Tucciarelli, T., ñAnisotropic potential of velocity ýelds in real þuids: Application to the MAST solution of shallow water equationsò, *Adv. Water Resour*., 62(Part A) (2013), pp.13-26.

(43) Kinjo, N., Yoshioka, H., Unami, K. and Fujihara, M., ñSimulation of water flows in an agricultural drainage system with hydraulic structuresò, *Proc. 2013 IAHR World Congress*, (2013), 12pp.

(44) Toro, E.F., *Riemann Solvers and Numerical Methods for Fluid Dynamics*, Springer, 2010, pp. 163-212.

(45) Fazãro, S.S. and Zech, Y., ñEffects of a sharp bend on dam-break flowò, *Proc. the 28th IAHR congress*, (1999), 7pp.

(46) Unami, K., Kawachi, T., Kranjac-Berisavljevic, G., Abagale, F.K., Maeda, S. and Takeuchi, J., ñCase study: Hydraulic modeling of runoff processes in Ghanaian inland valleysò, *J. Hydraul. Eng*., 135(7) (2009), pp. 539-553.

(47) Yoshioka, H., Unami, K. and Kawachi, T., ñAn upwind finite element scheme for stochastic contaminant particle dynamics in locally one-dimensional open channel networksò, *Proc. PAWEES 2011 International Student's Conference*, (2011), 16 pp.

(48) Ran, E., Yoshioka, H., Unami, K., and Fujihara, M., ñComputational fluid mechanics-based investigation of operational strategies for drainage gates installed in a polderò, *Proc. the Annual Meeting of Applied Hydraulics*, (2012), pp. 104-105. (in Japanese)

(49) Debsarma, S.K., ñSimulations of storm surges in the Bay of Bengalò, *Mar. Geod.*, 32(2) (2009), pp. 178-198.

(50) Lewis, M., Bates, P., Horsburgh, K., Neal, J. and Schumann, G., ñA storm surge inundation model of the northern Bay of Bengal using publicly available dataò, *Q. J. R. Meteorol. Soc*. 139(671) (2013), pp. 358-369.

(51) Chen, Y., Wang, Z., Liu, Z. and Zhu, D. (2012): ñ1Dï2D coupled numerical model for shallow-water flowsò, *J. Hydraul. Eng.*, 138(2) (2012), pp. 122ï132.

(52) Morales-Hernández, M., García-Navarroa, P., Burguete, J. and Brufau, P., ñA conservative strategy to couple 1D and 2D models for shallow water flow simulationò, *Comput. Fluids*, 81(20) (2013), pp. 26-44.

(53) Yoshioka, H., Takagi, K., Unami, K. and Fujihara, M., ñA horizontally 2-D shallow water model utilizing both the finite element and the finite volume techniquesò, *Proc. the 70^{th} Japanese Society of Irrigation, Drainage and Rural Engineering, Kyoto Division*, (2013), 2pp. (in Japanese, to appear)

(54) He, Z., Wu, W. and Wang, S.S.Y., ñCoupled finite volume model for 2D surface and 3D subsurface flowsò, *J. Hydraul. Eng*., 13(9) (2007), pp. 835-845.

(55) Xin, P., Yuan, L.R., Li, L. and Barry, D.A., ñTidally driven multiscale pore water flow in a creek-marsh systemò, *Water Resour. Res.*, 47(W07534) (2011), 19pp.

(56) Mishev, I.D., ñFinite volume methods on Voronoi meshesò, *Numer. Methods Partial Differ. Equat.*, 14(2) (1998), pp. 193-212.

(57) Yoshioka, H., Unami, K. and Fujihara, M., ñRelevant internal boundary conditions for the partial differential equations In locally one-dimensional open channel networksò, *Proc. the Annual Meeting of Applied Hydraulics in 2013*, (2013), 6pp. (to appear)

(58) Ishida, K., Yangyuoru, M., Unami, K. and Kawachi, T. ñApplication of shallow water equations to analyze runoff processes in hilly farmlandsò, *Paddy Water Environ*., 9(4) (2011), pp. 393-401.